CHEMICAL SENSORS AND INSTRUMENTATION POWERED

BY MICROBIAL FUEL CELLS

by

Raaja Raajan Angathevar Veluchamy

A thesis submitted in partial fulfillment
of the requirements for the degree

of

Master of Science

in

Chemical Engineering

MONTANA STATE UNIVERSITY
Bozeman, Montana

November 2007

APPROVAL

of a thesis submitted by

Raaja Raajan Angathevar Veluchamy

This thesis has been read by each member of the thesis committee and has been found to be satisfactory regarding content, English usage, format, citation, bibliographic style, and consistency, and is ready for submission to the Division of Graduate Education.

Dr. Joseph Seymour

Approved for the Department Chemical and Biological Engineering

Dr. Ron Larsen

Approved for the Division of Graduate Education

Dr. Carl A. Fox

STATEMENT OF PERMISSION TO USE

Raaja Raajan Angathevar Veluchamy

November 2007

ACKNOWLEDGEMENTS

TABLE OF CONTENTS

LIST OF TABLES

Table   Page

LIST OF FIGURES

LIST OF FIGURES - CONTINUED

NOMENCLATURE

R	$J\ K^{-1}\ mol^{-1}$	Universal gas constant
T	Kelvin	Temperature
[Red]	$mol\ m^{-3}$	Concentration of the reduced species
[Ox]	$mol\ m^{-3}$	Concentration of the oxidized species
n		Number of electrons transferred in the half-reaction
E_0	V	Standard half cell potential
E'	V	Half cell potential
$E'_{pH=7.2}$	V	Half cell potential based on a pH of 7.2
		Potential of the half cell with respect to the saturated
V_{SCE}	V	calomel electrode
Q	C	Charge accumulated in the capacitor
C	F	Capacitance of the capacitor
I	A	Average discharge current of the capacitor
t	s	Total discharge time
		Voltage across capacitor terminals at any instance of
V	V	time t
		Terminal voltage of the capacitor before start of
$V_{t=0}$	V	discharge
a		Integration constant
t_c	s	Lapse time after the controller starts operating

I_{avg}	A	Average current consumed
I_c	A	Current drawn by the controller
E_{avg}	Wh	Average energy consumption
$t_{lifetime}$	H	Lifetime of the probe
C_{Mg}	Ah/Kg	Capacity of the magnesium alloy based on manufacturer specification. (1111Ah/Kg)
W_{Mg}	Kg	Total weight of the magnesium anode used (10.8Kg)
I_{Active}	A	Average current drawn by the controller while active (0.163A)
I_{Sleep}	A	Average current drawn by the controller while in sleep mode (0.0043A)

ABSTRACT

The use of microbial fuel cells to power electronic devices is inhibited by their low voltage and current outputs, therefore they cannot be used directly to power electronic devices without appropriate power management. The goal of the thesis is to power chemical sensors but currently there are no available sensor circuitries which can be operated at the low potential and current delivered by a microbial fuel cell. In this thesis, novel sensor circuitry and power management circuitry have been developed. The sensor circuitry can be programmed to operate any generic amperometric sensor and the data is accessible using wireless communication. The power management circuitry boosts the low potential and current outputs of a microbial fuel cell to the higher level required for powering the sensor circuitry. For testing purposes, the sensor circuitry was programmed to operate a chemical sensor measuring copper and lead concentrations in water. This work has demonstrated that by adopting the proposed power management and sensor circuitry, the energy from a microbial fuel cell can be used for powering electronic devices, including chemical sensors deployed at remote locations.

INTRODUCTION

Project Background

The Biofilm Structure and Function Group at the Center for Biofilm Engineering at Montana State University-Bozeman was funded by the Office of Naval Research to perform research on the application of microbial fuel cells for powering remote sensors. In the initial phase of this project, microbial fuel cells were studied in the lab [1] which led to the development of a field deployable microbial fuel cell [2]. Although the microbial fuel cell developed by the research group was a reliable power source, its usefulness could not be realized since the existing chemical sensors could not be directly powered by the microbial fuel cells due to the low voltage and current output from the microbial fuel cell. The powering of a simple temperature sensor using a microbial fuel cell was first researched by Avinash Shantaram, one of the members of the Biofilm Structure and Function Group [3]. In Avinash Shantaram's thesis an off-the-shelf DC-DC converter and super capacitor were used to power a simple off-the-shelf temperature sensor. This off-the-shelf temperature sensor was able to wirelessly transmit the data over a few meters to a laptop. The power management was carried out by using a voltage comparator in the DC-DC converter chip. When the voltage across the super capacitor reached certain level, the voltage comparator was configured to enable the 5V output of the DC-DC converter. Once the 5V output of the DC-DC converter was enabled the temperature sensor

starts transmitting data periodically. In an effort to demonstrate that a more sophisticated sensor could be powered by using the power management strategy proposed by Avinash Shantaram, the potentiostat circuitry developed by the research group was powered by using the power management circuitry developed by Avinash Shantaram. But since the current requirements of the potentiostat were higher than the simple temperature sensor, changes in the power management strategy and the sensor circuit design were required in order to power the potentiostat circuitry using the microbial fuel cells.

Purpose

Over the last decade, microbial fuel cells have evolved from a conceptual lab device [4-9] to a practical power source that could be used to power sensors at remote locations [2]. Microbial fuel cells are high energy capacity devices which could provide low power output for many years without maintenance. This high energy capacity and reliability are highly desirable requirements for any power source, but microbial fuel cells have major drawbacks due to their low power output and their inability to be used in series configuration to obtain higher operating voltages. Series configuration does not work in the case of the microbial fuel cells deployed in the natural water systems due to the common electrolyte shared by the individual microbial fuel cells. Because of the common electrolyte (water), the anode and cathode interconnection between individual fuel cells, used in the series configuration, acts as a short circuit instead of

serving the intended purpose of adding the voltages from the individual fuel cells (Figure 1). These major drawbacks render microbial fuel cells less attractive for powering remote sensor electronics that are specifically designed for operation using a battery power source.
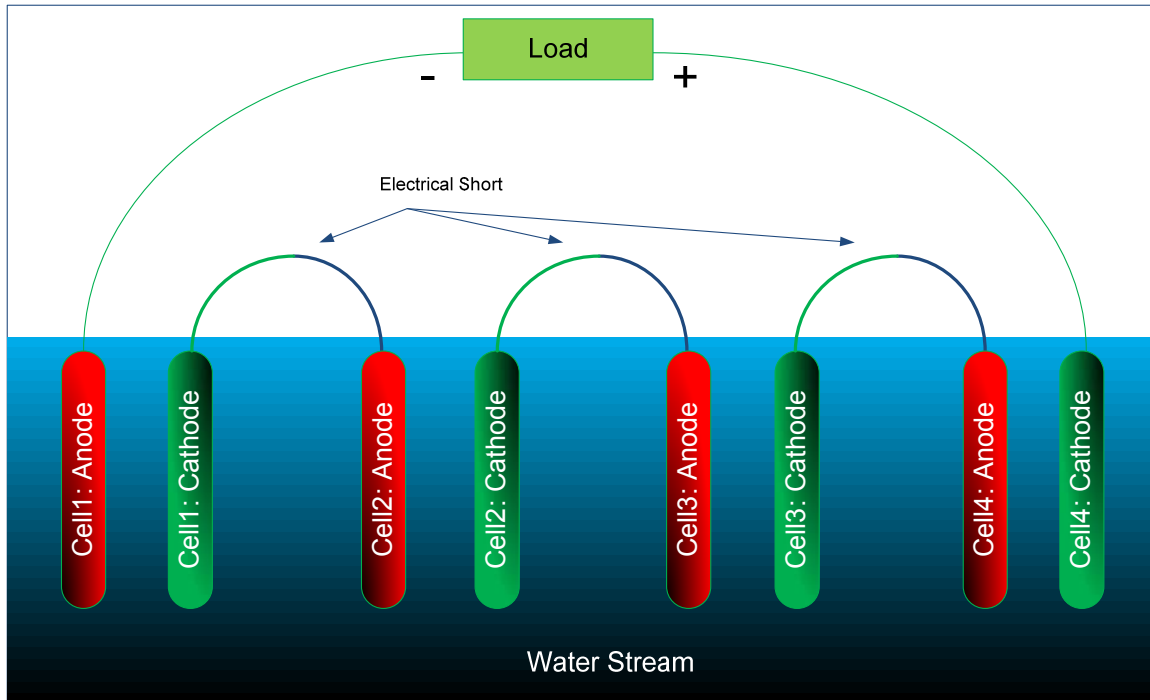
Figure 1. Pictorial representation of microbial fuel cells connected in series.

Since batteries are limited by the amount of energy they can store, researchers have mainly focused on designing sensor electronics which require low power for their operations and hence can be operated for longer durations using batteries. The design of these sensor electronics which consume low power also enables the deployment of these sensors at remote locations for longer durations with the need for less frequent visits to change batteries. Yun et al. developed a low power remote environmental monitoring system capable of

wirelessly transmitting the heavy metal concentration data to a base station [10]. That research group has used a wireless transmitter with a range of few meters and the type of power source used was not mentioned. Steinberg et al. developed a potentiostat that consumes very low power for its operation and could be used to operate analytical sensors [11]. Kwakye et al. developed an embedded system for usage in portable electrochemical analysis [12]. The embedded system developed was designed to operate on a 1.5V battery power, and the authors have claimed that it can be operated for 2 hours every day for up to 6 months. Although that system consumes low power, it does not find very much usefulness for remote environmental monitoring systems largely due to its requirement for a personal computer to log the data output by the sensor system. Using a personal computer indirectly implies that utility power is required, which totally voids the purpose of developing a low power remote sensor. Serra et al. have reported the design and construction of an amperometric biosensor with wireless capabilities [13]. That amperometric biosensor requires a battery pack for its operation and can transmit the data up to 30m. Beni et al. developed a portable sensor that measures the concentration of copper in the soil [14]. The runtime of that sensor was limited by the laptop used for the data logging. Reay et al. have reported an electrochemical analysis system to measure the concentration of lead and cadmium in aqueous solutions [15]. That system can be powered by batteries and is portable. The majority of the portable and remote sensor systems developed so far were operated using batteries, which was the

factor limiting their runtime. Also, in an effort to save energy consumption, the capabilities of the sensor systems were highly reduced. For example, most of the researches have resorted to using low power output wireless transmitters that can transmit data only a few meters. The bottom line is that the capabilities of the sensor system developed so far have been highly limited, mainly due to the power source constraints. Though these systems can technically be called remote sensors, their real world applications are very limited.

Since microbial fuel cells can be setup at remote locations where water resources exist, they are a convenient power source for remote environmental sensors. To make use of a reliable power source such as microbial fuel cells, in this work the design and development of the remote sensor circuitry which could be directly powered by microbial fuel cells is reported. The sensor circuitry can operate any generic amperometric sensor and transmit the response current data wirelessly to the base station. The sensor circuitry was tested by operating a sensor which could detect copper and lead concentrations in water samples. The sensor circuitry consists of a potentiostat circuitry, a power management circuitry, and a wireless transmitter. The potentiostat circuitry, power management circuitry and the wireless transmitter together, are referred to as a "controller" in the remaining part of this thesis. The controller, the microbial fuel cell and the sensor are collectively referred to as a "probe". In this work, the main focus is on the design, construction, and testing of the potentiostat and the power management circuitry. Figure 2 shows the pictorial representation of the system used to test

the controller developed in this work. Figure 3 is the simple block diagram version of the complete system shown in Figure 2.
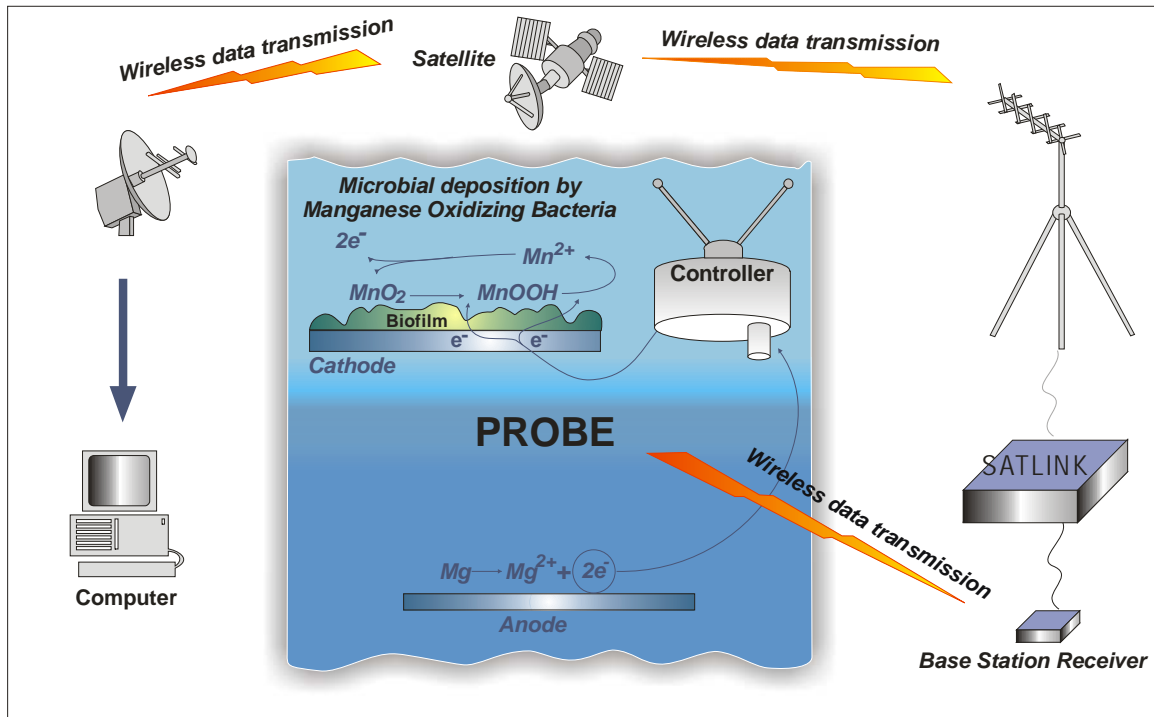
Figure 2. Pictorial representation of the complete system used for testing the controller. The controller consists of potentiostat circuitry, a wireless transmitter and power management circuitry. The probe consists of a sensor, a microbial fuel cell and the controller. The data transmitted by the probe is received by the base station receiver and then sent to the satellite using a Stalink® wireless transmitter. The data sent to the satellite can be accessed from a database server using a computer.

Goal

Develop and test a controller which can be powered by a microbial fuel cell.
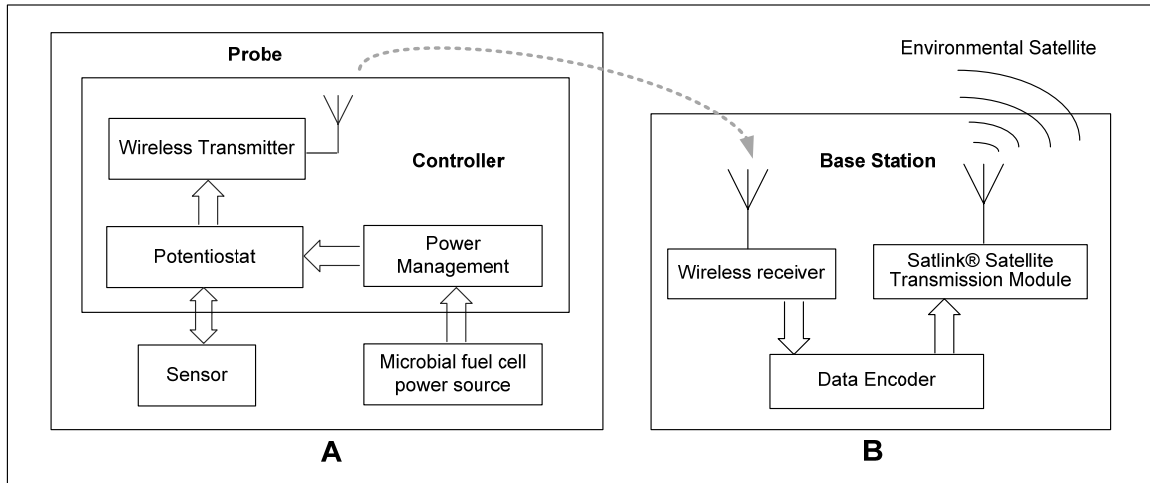
Figure 3. A. Simplified block diagram of the probe; B. Simplified block diagram of the base station.

Challenges

1. Microbial fuel cells cannot output the current and voltage required to operate the electronic components used in the controller.

2. There is no potentiostat circuitry available which can be powered by a microbial fuel cell.

To overcome these challenges, the following tasks and strategies were employed.

Tasks

1. Design potentiostat circuitry.

2. Design power management circuitry.

3. Construct thin film mercury electrode which can be used to perform anodic stripping voltammetry.

4. Operate the thin film mercury sensor using a commercial potentiostat and the potentiostat developed in this thesis.

Strategy

1. Use super capacitor to store the electrical energy output by the microbial fuel cell and to supply the high current required to operate the sensor circuitry.

2. Use DC-DC converter to step up the voltage of the microbial fuel cell.

3. Use a supervisory microcontroller to periodically monitor the amount of energy accumulated in the super capacitor and turn on the potentiostat when enough energy is accumulated to perform one full anodic stripping voltammetry (ASV) sequence.

4. To conserve power, use a separate DC-DC converter for powering the potentiostat and the power management circuitry. In this arrangement, the DC-DC converter powering the potentiostat can be completely turned off which lowers the continuous power requirement considerably.

5. Integrate the custom designed potentiostat with a long range wireless data transmitter.

Microbial Fuel Cells

A microbial fuel cell is an electrical power source which uses microbes as a catalyst to convert chemical energy into electrical energy [16]. Microbial fuel

cells can be configured in different ways depending on the type of anodic and cathodic reaction. The microbial fuel cell used in this work consisted of a sacrificial anode combined with cathodic reduction of biomineralized manganese oxide [2]. The sacrificial anode used was an alloy composed mainly of magnesium. The other metals present in the alloy help passivate the magnesium and therefore lower its dissolution rate to prolong its life. The anodic and cathodic reactions occur according to Equation 2 and Equation 3, respectively. Equation 3 occurs in two steps; first, biomineralized manganese dioxide is reduced to produce manganese oxyhydroxide (Equation 4), and then the manganese oxyhydroxide is further reduced to produce divalent magnesium ions (Equation 5). The divalent magnesium ions (Equation 5) are electrodeposited by microbial action. The potentials in Equation 2 to Equation 5 were calculated using Nernst equation (Equation 1).

$$E^{'} = E_0 - \frac{RT}{nF} \ln \frac{[Red]}{[Ox]}$$

Equation 1

$Mg \Rightarrow Mg^{2+} + 2e^-$ $\qquad E'_{pH=7.2} = -2.105\ V_{SCE}$ Equation 2

$MnO_2(s) + 4H^+ + 2e^- \Rightarrow Mn^{2+} + 2H_2O$ $\qquad E'_{p\ H=7.2} = +0.36\ V_{SCE}$ Equation 3

$MnO_2(s) + H^+ + e- \Rightarrow MnOOH(s)$ $\qquad E'_{pH=7.2} = +0.383\ V_{SCE}$ Equation 4

$MnOOH(s) + 3H^+ + e^- \Rightarrow Mn^{2+} + 2H_2O$ $\qquad E'_{pH=7.2} = +0.336\ V_{SCE}$ Equation 5
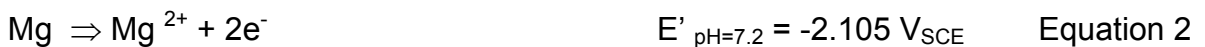
Sensor Theory

The sensor used in this work was operated using anodic stripping voltammetry (ASV), which is a well known electroanalytical technique commonly used for determining heavy metal concentrations in water samples [17-22]. Using precision instrumentation measuring low level currents, concentration levels of parts per billion of metal ions present in the water samples can be determined. ASV consists of two discreet steps (Figure 4). First, the metal ions present in the water sample are electrodeposited on a thin film of mercury by applying a negative potential at the working electrode with respect to the reference electrode. Then, the potential of the working electrode is scanned towards a positive potential with respect to the reference electrode. During the scanning peaks are observed at certain stripping potentials. Each metal has different stripping potential. The stripping potentials for copper and lead are $185mV_{SCE}$ and $-430mV_{SCE}$ respectively. A calibration curve can be prepared by measuring the peak current for different concentrations of the metal present in the water sample. Initially, ASV was carried out using a dropping mercury electrode [23] as the working electrode, but the latest advancements involve a thin film mercury electrode [24] and ultramicroelectrodes as the working electrode [25]. This reduces the mercury requirement and also makes it an attractive option for environmental water pollution monitoring. For this research, thin film mercury

electrodeposited over a graphite surface was used to detect copper and lead concentrations.
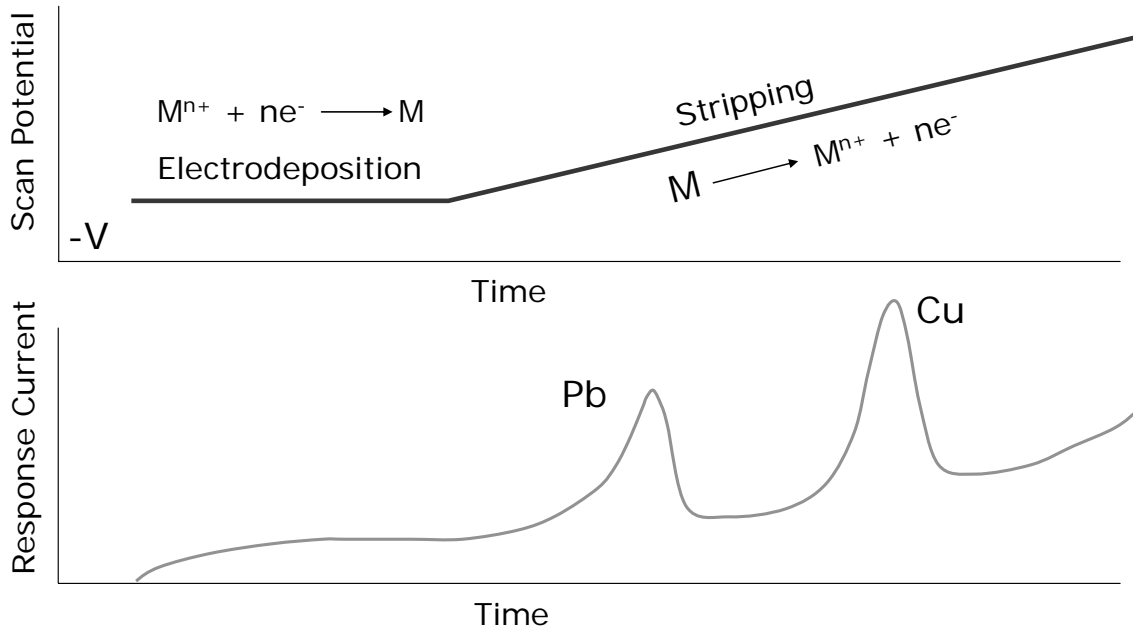
Figure 4 The scan potential verses time plot shows the potential applied by the potentiostat on the working electrode with respect to the reference electrode. M^{n+} is any metal ion present in the water sample. Response current verses time plot shows the response current corresponding to the scan potential generated by the potentiostat. Current peaks from copper and lead are shown as examples.

Sensor Instrumentation Theory

Chemical sensors can be broadly classified as potentiometric or amperometric sensors. For operating potentiometric sensors, an excitation current is required, and the response is obtained as a voltage signal. For operating amperometric sensors, an excitation voltage has to be supplied, and the response is obtained as current signal. The instrumentation required to operate an amperometric sensor is called a potentiostat. The instrumentation

required to operate a potentiometric sensor is called a galvanostat. In this work, the type of sensor instrumentation developed is a potentiostat that could be programmed to operate amperometric sensors. In order to operate the ASV sensor used in this thesis, the potentiostat's microcontroller was loaded with a program that performs ASV sequence. By changing the program loaded in the potentiostat's microcontroller, different types of amperometric sensors can be operated by the potentiostat. Measuring very low concentrations of heavy metal ions using ASV requires high precision instrumentation. In this work, by using a combination of high precision analog and digital integrated circuits, the potentiostat developed was able to perform ASV with a high degree of accuracy. The response current values from ASV were digitized. This facilitated the wireless transfer of data to the base station using digital mode. Use of digital data transmission increased reliability over longer distances when compared to analog data transmission.

Increasing the Potential Output by the Microbial Fuel Cell

Integrated circuit chips used in the controller required a minimum of 5V for operation. The useful operating voltage of the microbial fuel cell used in this work can range anywhere between 0.8 V and 2.1 V. The effect of high electrical resistance of natural water combined with variations in microbial activity is the main factor affecting the operating voltage output by the microbial fuel cell. For stepping up the voltage of the microbial fuel cell, a DC-DC converter circuit was

used. This DC-DC converter was able to output the 5V required for the operation of the sensor instrumentation, the wireless transmitter, and the power management microcontroller.

Storing Energy

The power requirements of the potentiostat and the wireless transmitter were met by storing energy in a super capacitor. A capacitor which has very high storage capacity and very low leakage current is called a super capacitor. When the sensor is not operational, the electrical energy produced accumulates in the capacitor. Super capacitors can output a current that is many times greater than the microbial fuel cell's output current. With the super capacitor being the major contributor, the current output by the super capacitor and microbial fuel cell together is used to operate the controller. Use of the super capacitor makes it possible to calculate the amount of energy accumulated by knowing the terminal voltage. This makes it easier for the power management circuitry to determine if enough energy has been accumulated in the super capacitor to perform one full ASV sequence and wireless transmission.

14

MATERIALS AND METHODS

Overall Functional Description of the System

The detailed block diagram of the sensor system consisting of the probe
and the base station is shown in Figure 5. The master microcontroller in the
power management circuitry (Figure 5 A) determines when to turn on the
potentiostat circuitry (Figure 5 A.f). The master microcontroller constantly
monitors the voltage across the super capacitor (Figure 5 A.b). Whenever the
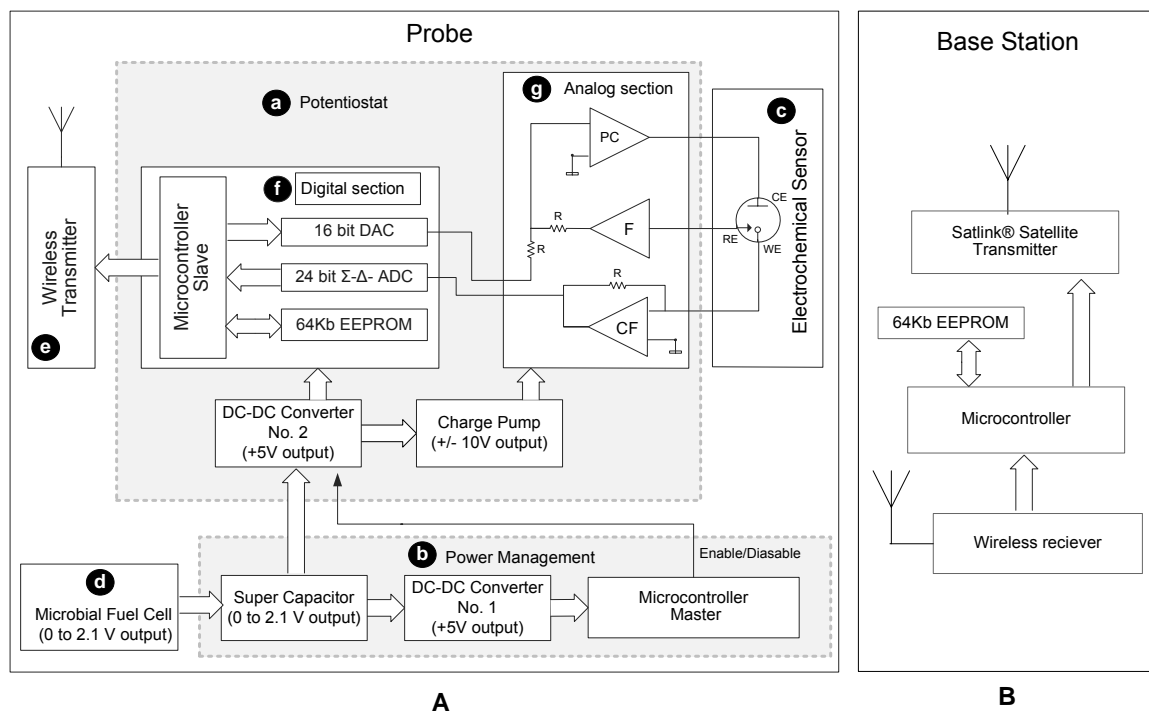
Figure 5. Detailed block diagram of the complete system consisting of the probe
(A) and the base station (B). (RE = Reference electrode, WE= Working
electrode, CE= Counter electrode, PC=Potential controller, F=Voltage follower,
CF=Current follower).

super capacitor accumulates enough charge to perform one ASV scan and wireless transmission, the master microcontroller turns on the power to the potentiostat circuitry by enabling the DC/DC converter No.2 (Figure 5 A.a). Once powered up, the potentiostat circuitry starts performing the ASV sequence and then transmits the data wirelessly using the wireless transmitter (Figure 5 A.e). To conserve power, the wireless transmitter stays in sleep mode unless enabled by the potentiostat circuitry for the wireless data transmission. After the wireless transmission, the slave microcontroller in the potentiostat informs the master microcontroller (Figure 5 A.b) that the ASV data transmission is finished. The master microcontroller shuts down the power to the potentiostat circuitry and waits until the super capacitor accumulates enough charge for performing another ASV scan and wireless transmission. The microcontroller at the base station (Figure 5 B) receives the data from the wireless receiver and delivers it to the data buffer memory of the satellite transmitter. The satellite transmitter sends the data to the satellite at the programmed time window every day. The data can be accessed from the central satellite database website.

<div align="center">Potentiostat</div>

The potentiostat circuitry (Figure 5 A.a) has a digital and analog section. The analog section (Figure 5 A.g) was constructed using high precision operational amplifiers [23]. The digital section (Figure 5 A.f) was composed of an analog to digital converter (ADC), digital to analog converter (DAC), and slave

microcontroller. The function of the potential control (PC) operational amplifier is to maintain the potential between the reference electrode and the working electrode equal to the potential output by the DAC. The PC carries out this function by varying the current flowing through the working electrode and the counter electrode. The PC is used in a potential adder configuration. The voltage follower (F) serves as a buffer so that only very small current is drained from the reference electrode. The operational amplifier configured as a voltage amplifier and inverter serves as a current to voltage converter (CF). CF makes it possible to read current in terms of voltage. The voltage output by the CF is proportional to the current flowing through the counter electrode and the working electrode. The voltage output by the voltage follower, which is equal to the response current, is converted to digital codes by the ADC. These digital data are sequentially stored in the electrically erasable programmable read only memory (EEPROM). Once the ASV sequence is finished, the response current data stored in the EEPROM are transmitted to the base station.

<u>Microbial Fuel Cell</u>

The microbial fuel cell was deployed in the Hyalite Creek, in Bozeman, MT. Twelve magnesium-alloy rods (Farwest Corrosion Control Company, Gardena, CA 90248) connected in parallel were used as anodes. The anodes were partly buried at the bottom of Hyalite Creek. The magnesium-alloy anode developed a potential of $-1.6V_{SCE}$ in the Hyalite Creek water. The cathode was

made up of 316L stainless steel wire. Stainless steel wire balls were enclosed in a wooden frame and then immersed in the water stream. This arrangement was left in the water for several days so that microbial activity could develop at the cathode. The stainless steel wires developed an open circuit potential of about 428mV$_{SCE}$ when deployed in Hyalite Creek water.

<u>Electrochemical Sensor</u>

The working electrode was fabricated by electrodepositing mercury on a glassy carbon electrode (3mm X 150mm Sigma Aldrich 496545-60G, CAS 7782-42-5). The glassy carbon electrode was masked using Teflon tape so that the mercury electrodeposition occurred over 40mm length of the electrode. Solution containing 1ppm of Hg^{2+} was used as the electrolyte for the mercury electrodeposition. The electrolyte was prepared by dissolving mercurous nitrate dihydrate (Sigma Aldrich #230413, CAS 7782-86-7) in deionized water containing 5% (w/w) concentrated nitric acid. Electrodeposition was carried out by applying a potential of -0.9 V$_{SCE}$ on the glassy carbon electrode using a Princeton Research EG&G 237A potentiostat for 1 minute. A glassy carbon electrode was used as the counter electrode.

The ASV sensor was assembled by fixing the thin film mercury electrode, saturated Ag/AgCl reference electrode, and graphite counter electrode in a rubber stopper with appropriate holes drilled (Figure 6). The whole assembly was

enclosed in a PVC tube with an open end. The sensor was deployed by submerging the open end of the PVC casing in the water.
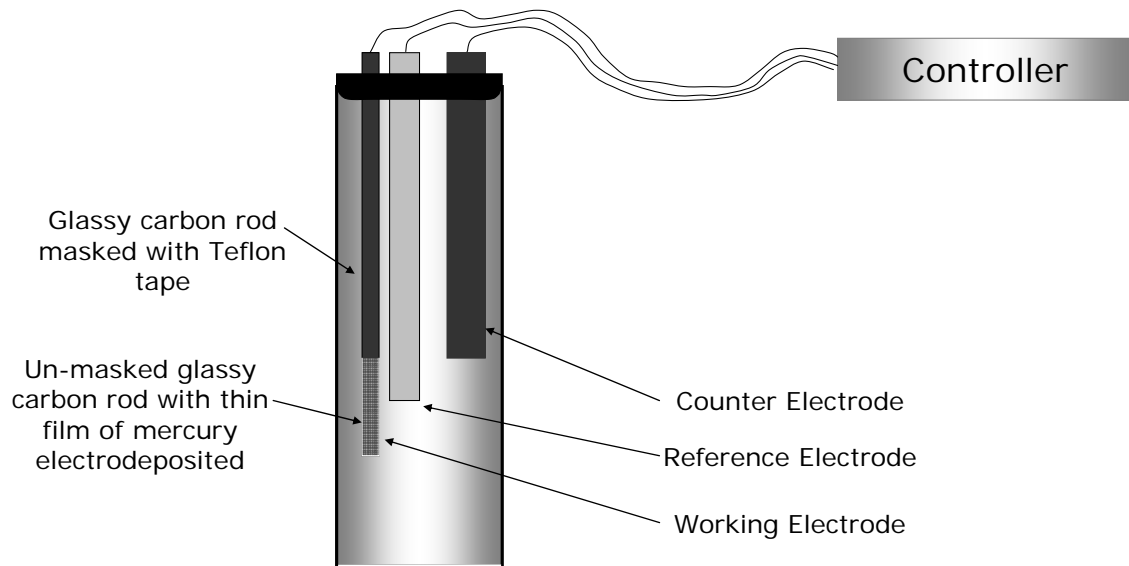
Figure 6. ASV sensor assembly.

Detailed Controller Circuit Description

Analog to Digital Conversion

Figure 7 shows the detailed circuit diagram of the analog to digital conversion section of the potentiostat. The ADC (Figure 7) was supplied with the voltage signal from the current follower (Figure 9: I_TO_V), and the voltage signal was converted to a 24bit digital code. Since the voltage signal output by the current to voltage converter was in the range of -4V to +4V, a voltage level converter (Figure 7: ADC_BIP_CONV) was used to convert it to the 0 to 4V range. For analog to digital conversion to occur, the ADC had to be supplied with

a clock signal (CLK). The clock signal was generated using the µC3 micro controller (Figure 7).
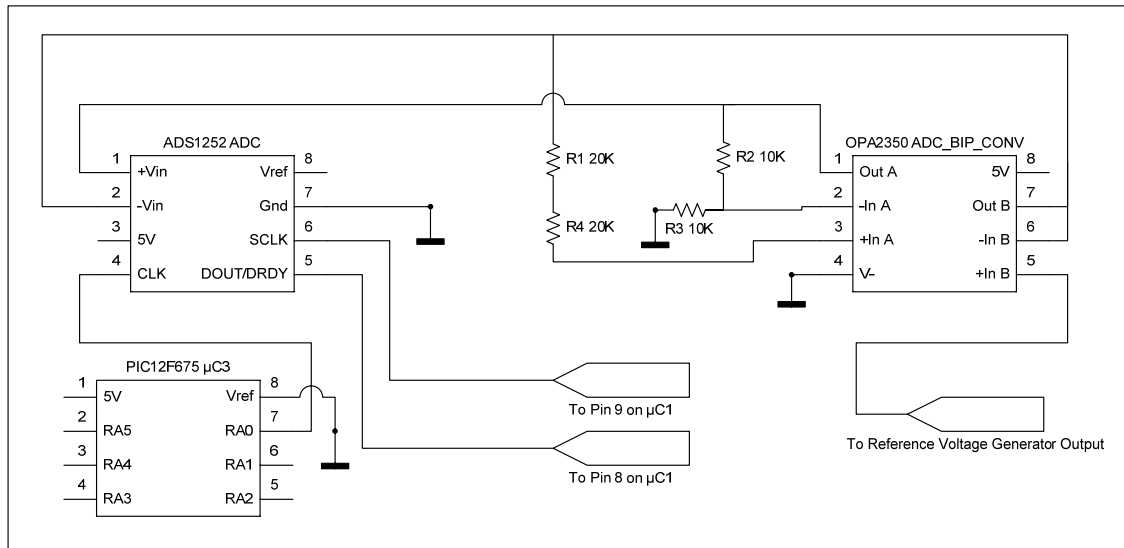
Figure 7. Circuit diagram of the analog to digital conversion section of the potentiostat.

Digital to Analog Conversion

The 16bit digital code supplied to the digital to analog converter (Figure 8: DAC) was converted to an analog signal in the range of 0 to 5 V. Since the ASV scanning process involved negative and positive potentials, the DAC was coupled with operational amplifier (Figure 8: ADC_BIP_CONV) to generate -2.5V to +2.5V bipolar outputs.

Analog Section

The analog section of the potentiostat was constructed using operational amplifiers. To minimize the amount of current drawn from the reference electrode, the REF_BUF (Figure 9) was wired as a voltage follower. The I_TO_V

(Figure 9) was wired as a current follower, which performed the function of converting the response current to equivalent voltage signal. The ADDER, configured as a potential adder, performed the function of maintaining the potential between the reference electrode and the working electrode equal to the voltage output by the DAC. The detailed circuit diagram of the analog section of the potentiostat is shown in Figure 9.
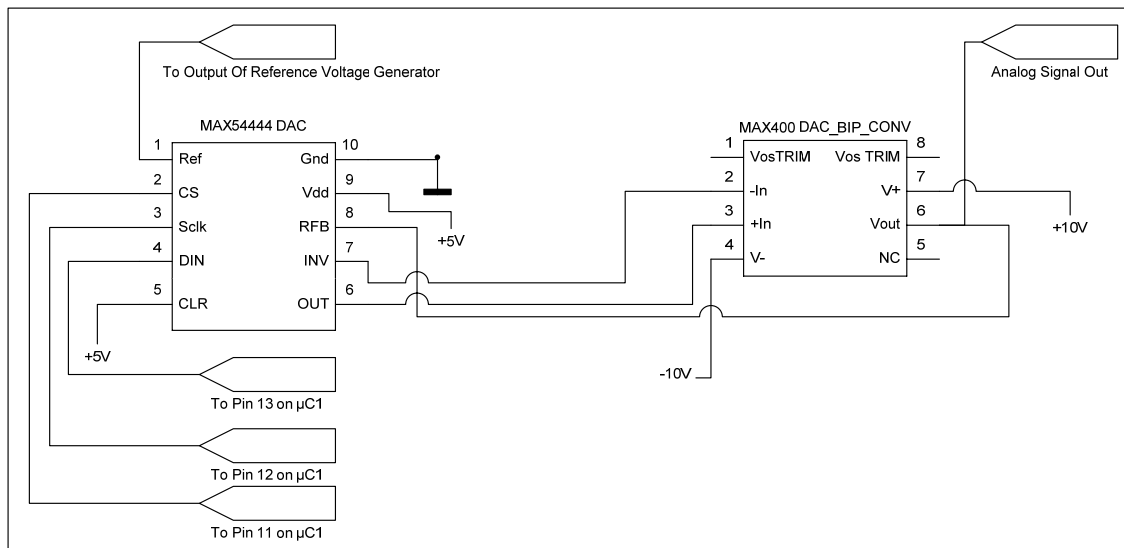
Figure 8. Circuit diagram of digital to analog conversion section.

EEPROM

Figure 10 shows the wiring diagram of the EEPROM to the µC1 microcontroller. During the ASV sequence, response current values were stored in the EEPROM1 (Figure 10). Current values stored in the EEPROM1 were delivered to the wireless transmitter after the ASV sequence was finished.
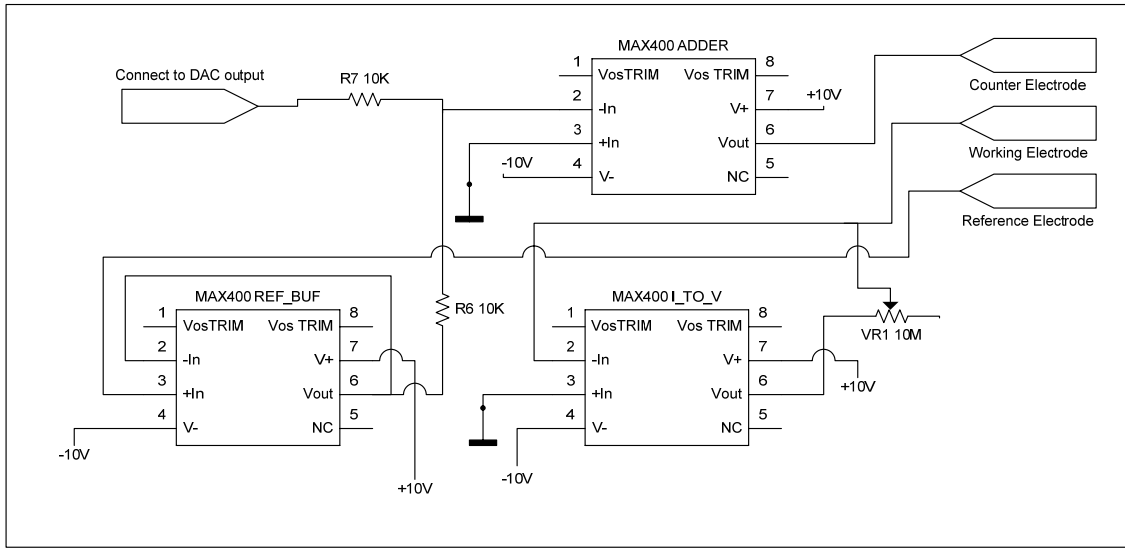
Figure 9. Analog section of the potentiostat.
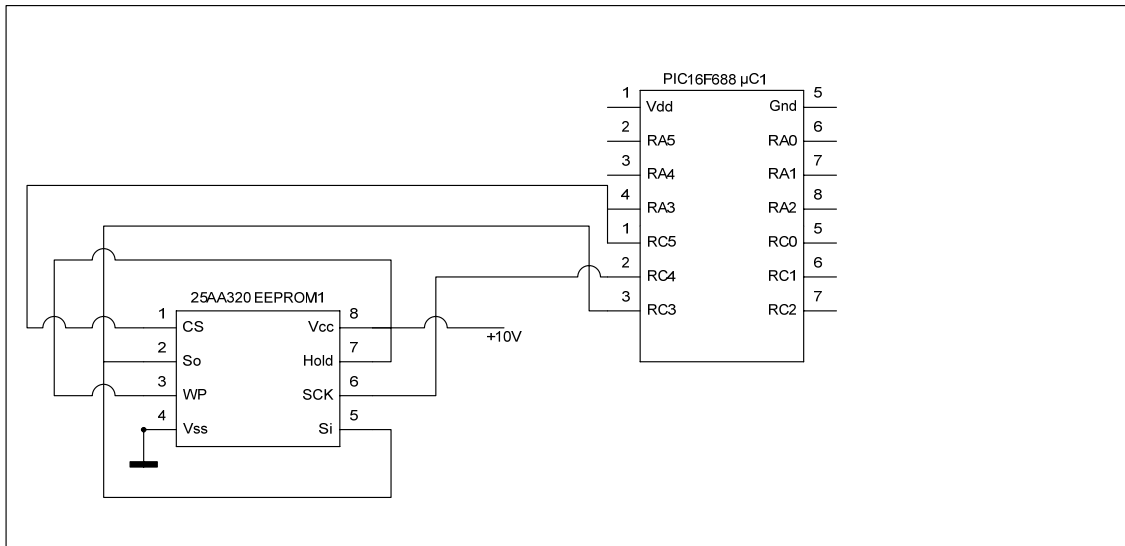
Figure 10. Wiring diagram of EEPROM to the µC1.

Reference Voltage Generator

The DAC and the ADC required stable accurate reference voltage for proper functioning. This reference voltage was generated using the circuit given

in Figure 11. A REC3140 (Figure 11) generated the highly stable voltage that was coupled with the voltage buffer to produce a highly stable reference voltage.
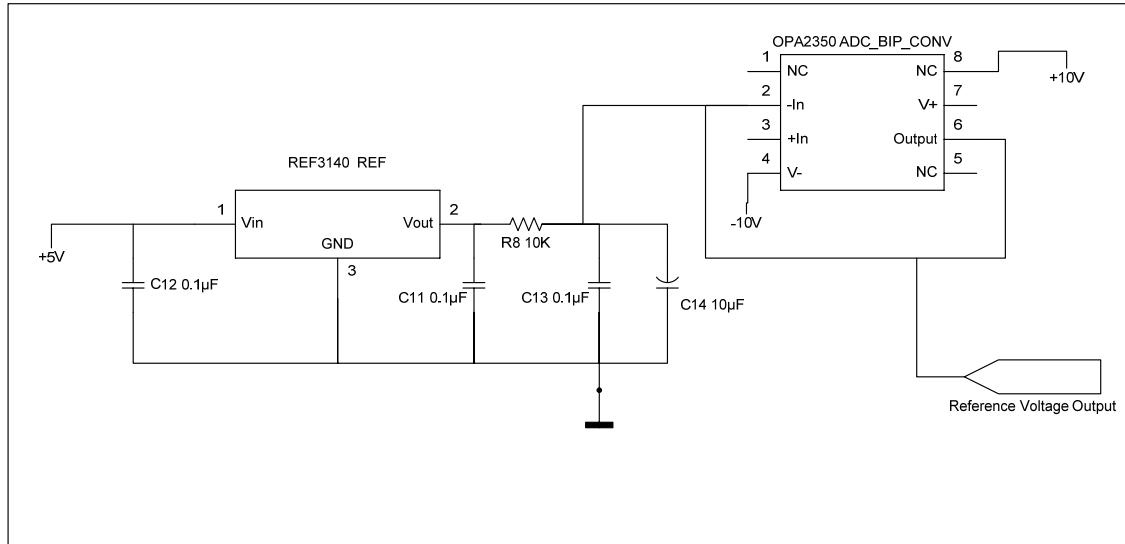
Figure 11. Detailed circuit diagram of the reference voltage generator.

Charge Pump

Figure 12 shows the detailed circuit diagram of the charge pump. Two charge pumps were wired in parallel to generate ±10V and up to 20mA of current. The voltage output of the charge pumps was used to operate the operational amplifiers in the analog section of the potentiostat.

Power Management

Figure 13 shows the detailed circuit diagram of the power management section of the controller. The electrical energy produced by the microbial fuel cell was stored in the super capacitor (SC). The voltage across the SC gradually increased with increases in the amount of energy stored. The comparator in DC1
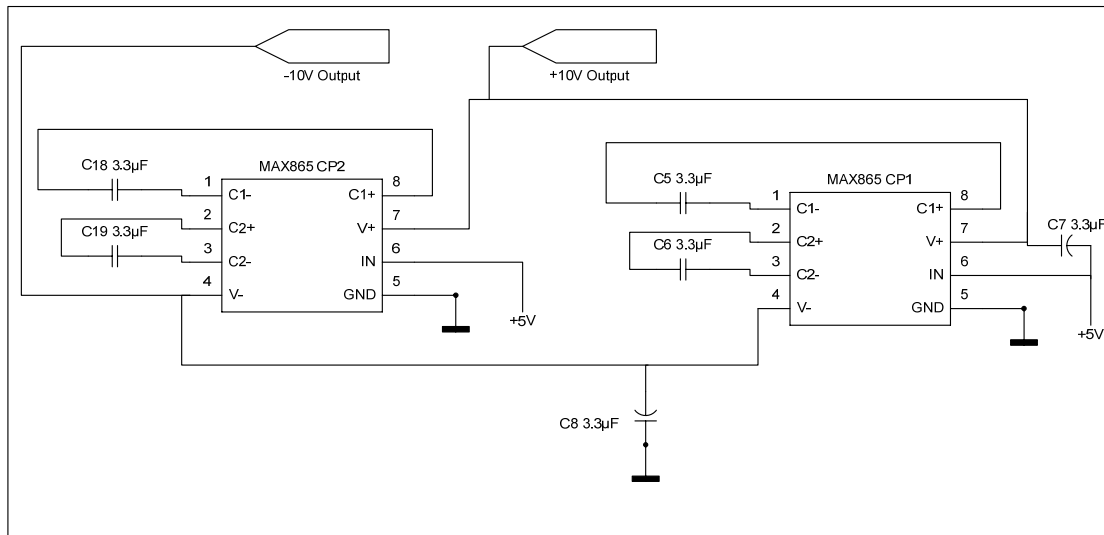
Figure 12. Detailed circuit diagram of the charge pump.

(Figure 13) was configured to enable its output as soon as the voltage across the SC reached 1.1V. The voltage at which the DC1 would enable its output was set using the VR2 (Figure 13). When the DC1 enabled its output (5V), the μC2 (Figure 13) was powered up and started the execution of the ASV sequence program stored in its flash memory. The program in μC1 (Figure 13) constantly polled the voltage across the super capacitor. When the voltage across the super capacitor reached 1.4V, the DC2 (Figure 13) output was enabled by sending signal high to the SHDN pin of the DC2, and then the program in the μC2 stopped execution until Pin10 went high. Once the DC2 powered the μC1, the program stored in the μC1 was executed. The program in μC1 performed the ASV sequence, the data transmission using wireless transmitter, and then sent the high signal to Pin10. As soon as Pin10 went high, the program in the μC2 disabled the DC1 output and then waited for 24 hours before enabling the DC1 output.
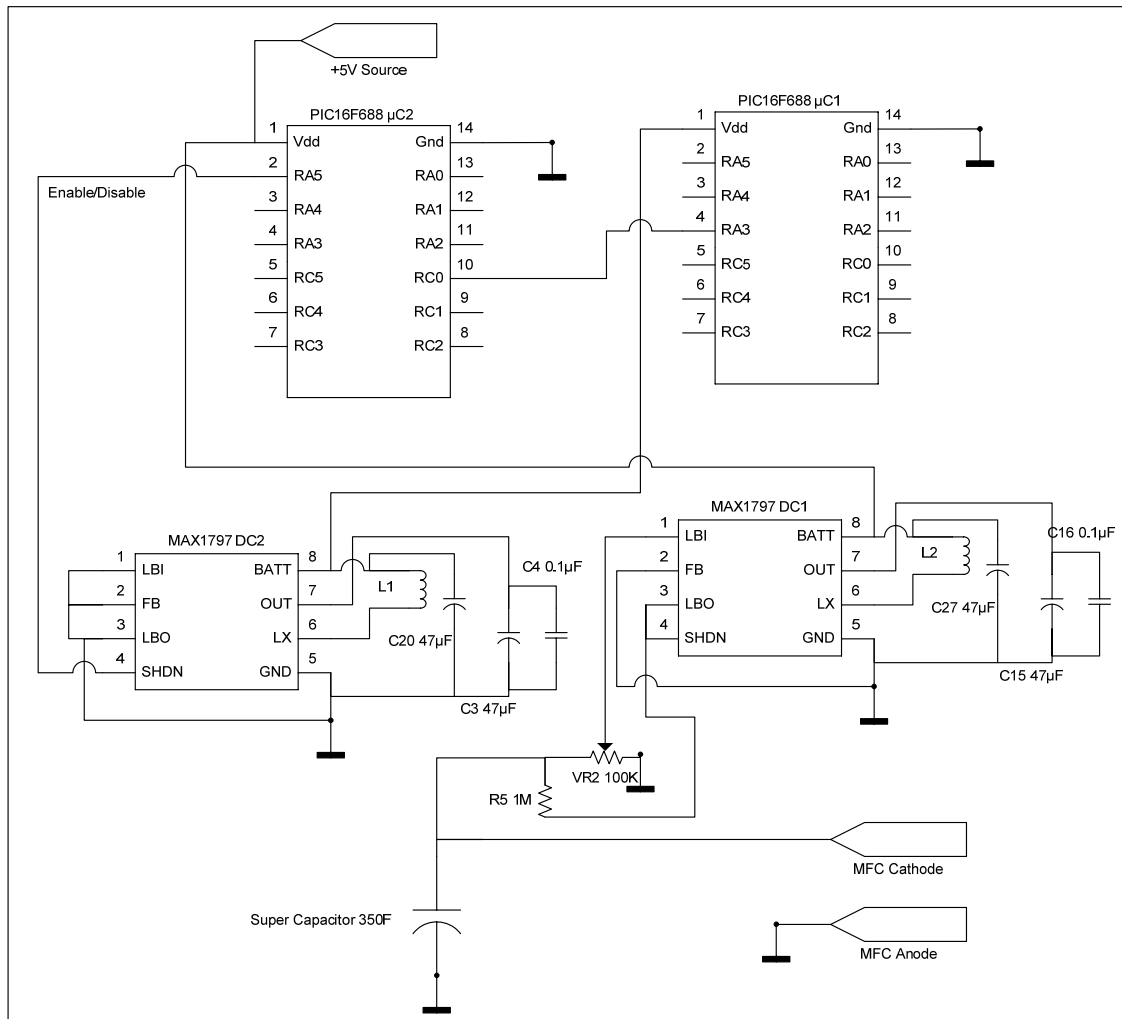
Figure 13. Detailed circuit diagram of the power management circuitry.

Controller Circuit Board Construction

The circuit layout and the PCB layout was done using ExpressSCH and Express PCB respectively, both supplied by www.expresspcb.com . In order to reduce the PCB fabrication cost and also to make a compact PCB, a two sided PCB design was used. The components were placed in a manner to make a smaller PCB. Once the component placement was finished the circuit layout file

was linked to the PCB layout file. This linking helped in connecting the components using the connection aid feature present in the ExpressPCB software. Most of the PCB tracks connecting the components were placed on the component side. Those tracks, which cannot be laid without crossing the other tracks, were placed on the bottom side of the PCB layout. The complete controller circuit diagram and the controller PCB layout are shown in

Figure 15 and Figure 16 respectively. The detailed base station circuitry and the base station PCB layout are given in Figure 14 and Figure 17 respectively. Once the PCB layout was finished, it was submitted online to www.pcbexpress.com for fabrication. Figure 16 shows the PCB layout of the controller created using ExpressPCB software.

Figure 17 shows the PCB layout of the base station circuitry. Green on the PCB layout represents the bottom side of the PCB. Red represents the top side (component side) of the PCB.

The microcontrollers were mounted to the circuit board using a socket for easy removal and insertion. This helped in the developmental phase when the microcontroller had to be removed for software updates. The electronic components were mounted on the PCB using low temperature solder (300°C). All of the integrated circuits (IC) used were surface mounted except for the microcontrollers which were mounted using sockets. Once the circuit layout was finished, the first step in the PCB layout was to decide the placement of the active components.

Figure 14. Complete circuit diagram of the base station.

The master and slave microcontrollers (PIC12F688) were supplied by Microchip Technology Inc, Arizona, USA. The DC-DC converters were based on MAX1797 supplied by Maxim Integrated Products, Sunnyvale, CA. The ADC (ADS1252, Texas Instruments) had a resolution of 24bits and was supplied by Texas Instruments, Dallas, TX. The DAC was based on MAC5442 (Maxim) which had a resolution of 16 bits. The analog section was constructed based on ultra low offset voltage operational amplifiers MAX400 supplied by Maxim Integrated Products, Sunnyvale, CA. The charge pump used to generate the ±10V supply voltage for the analog section was based on MAX865 (Maxim). A more comprehensive list of components used is given in Table 1.

Table 1. List of components used to construct the controller board.

Component Name Abbreviation	Component	Part Number/ Datasheet Reference	Source
DAC	Digital to Analog Converter	MAX54444 [26]	Maxim Integrated Products, Inc., Sunnyvale, CA USA
DC1, DC2	DC-DC Converter	MAX1797 [27]	
CP1, CP2	Charge Pump	MAX865 [28]	
DAC_BIP_CONV, ADDER, REF_BUF, I_TO_V	Operational Amplifier	MAX400 [29]	
ADC_BIP_CONV	Operational Amplifier	OPA2350 [30]	Texas Instruments Inc., Dallas, Texas, USA
ADC	Analog to Digital Converter	ADC1252 [31]	
µC1, µC2, µC4	Micro Controller	PIC16F688 [32]	Microchip Technology Inc., Chandler, Arizona, USA
EEPROM1, EEPROM2	Electrically Erasable Programmable Read Only Memory	25AA320 [34]	

Table 1-Continued

TX, RX	Radio Modem	9XTend	MaxStream, Inc., Lindon, Utah, USA
SC	Super Capacitor	BCAP0350	Maxwell Technologies Inc., San Diego - USA
C1, C2, C4, C22, C9, C12, C11, C14, C10, C16	Capacitor	0.1µF	Generic
C20, C3, C21, C15	Capacitor	47 µF	Generic
C18, C19, C5, C6, C8, C7	Capacitor	3.3µF	Generic
C13	Capacitor	10µF	Generic
R1, R2, R8, R6, R7, R3	Resistor	10KΩ	Generic
R9	Resistor	68KΩ	Generic
R4	Resistor	20KΩ	Generic
R5	Resistor	1MΩ	Generic
VR1	Variable resistor(10 turn)	1MΩ	Generic
VR2	Variable resistor(10 turn)	100KΩ	Generic
L1, L2	Inductor (surface mount)	22µH	Generic
µC3	Micro Controller	PIC12F675 [33]	

Figure 15. Schematic representation of the controller circuit.
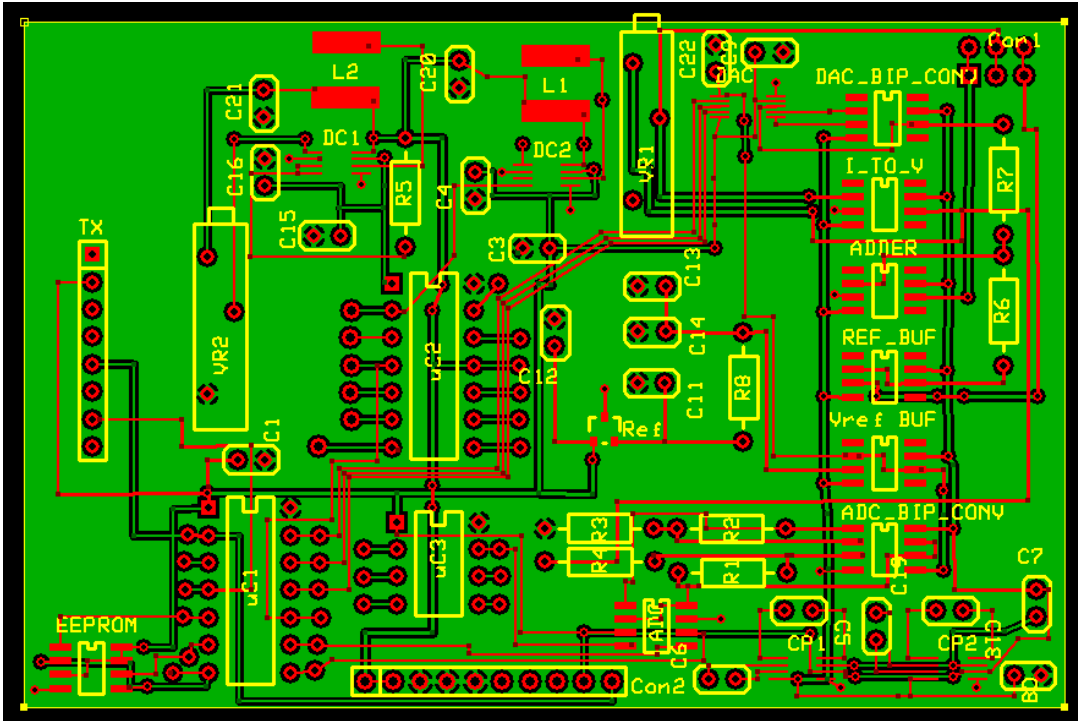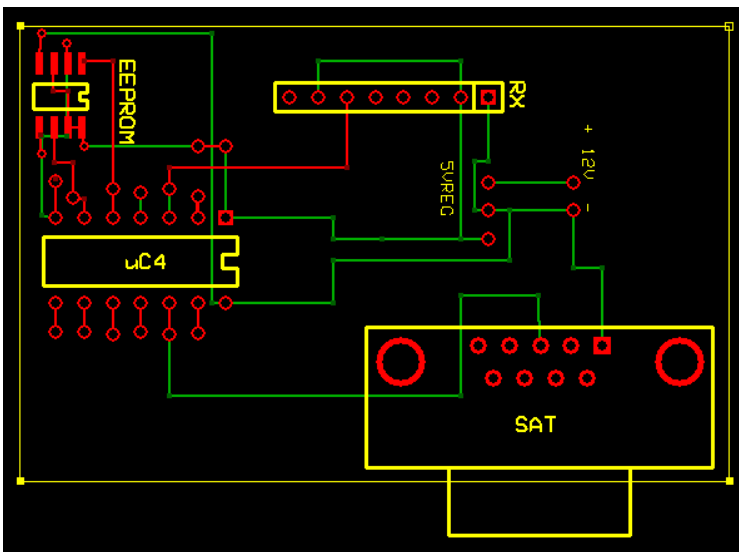
Figure 16. PCB layout of the controller.

Figure 17. PCB layout of the base station circuitry.

Wireless Transmitter

The radio modem used for wireless transmission and reception of the data from the potentiostat to the base station was based on the long range OEM RF module 9XTend (Maxstream Inc, Lindon, UT). To conserve power, the radio modem in the potentiostat was configured to the "transmission only" mode, while the radio modem in the base station was configured to the "receiver only" mode. The data were sent to the satellite using Satlink2 Multi-Satellite transmitter manufactured by Sutron Corporation, Sterling, VA. The Satlink2 module had 4 kb of transmit buffer memory. Data received by the Satlink2 were temporarily stored in the transmit buffer until the next transmission time window. Data transmitted to the satellite were cleared after the transmission. The data received by the environmental satellite were sent to the file transfer protocol (FTP) server. The data from the FTP could be accessed using the FTP client program supplied by Sutron Corporation, Sterling, VA. The FTP program collected and saved the data as text files.

Storing Energy and Capacitor Selection

The correct size (Farad) of the super capacitor had to be used for accumulating the energy output by the MFC. An oversized capacitor would take a long time to get charged up to the operating voltage of the sensor circuitry. An undersized capacitor would not have enough charge to deliver the required

current/potential for the length of time the controller required power. The discharge current of a capacitor is related to the rate of removal of charge from the capacitor according to the Equation 6. The amount of charge (Q) accumulated in the capacitor is related to the voltage and the capacitance according to the Equation 7. Substituting for Q from Equation 7 into Equation 6 we get Equation 8. Equation 8 upon rearrangement and integration yields Equation 10. The value of the integration constant can be obtained by setting t=0 and V=$V_{t=0}$. Substituting Equation 11 into Equation 10 and rearranging yields Equation 12. Further simplification of Equation 12 yields Equation 13.

$$I = \frac{dQ}{dt}$$ Equation 6

$$Q = VC$$ Equation 7

$$I = -\frac{d(V \times C)}{dt}$$ Equation 8

$$I = -C\frac{dV}{dt}$$ Equation 9

$$I \times t = -C \times V + a$$ Equation 10

$$V = C \times V_{t=0}$$ Equation 11

$$V = \frac{C \times V_{t=0} - I \times t}{C}$$ Equation 12

$$V = V_{t=0} - \frac{I \times t}{C}$$ Equation 13

The capacitor size can be estimated using Equation 13. To estimate the capacitor size, $V_{t=0}$ is set to 1.5V, the voltage at which the ASV sequence is

started by the sensor circuitry. V is set to 1V, which is slightly higher than the minimum voltage required for the proper functioning of the sensor circuitry. Average discharge current (I) is set to the average current drawn by the sensor circuitry, 0.5A. Total discharge time (t) is set to 160s, the time required to perform one complete ASV sequence and data transmission. For the selected parameter values, the value of capacitance of the capacitor (C) equals 266F. The super capacitor available from Maxwell technologies in this range has a capacity of 350F, which was used in the power management circuitry described in this paper. The leakage current for the capacitor selected is 300μA. Equation 13 does not take into account the voltage drop (IxR_{int}) due to the internal resistance of the capacitor, where R_{int} is the internal resistance of the super capacitor. In the case of the super capacitor, R_{int} is very small, and thus, the voltage drop due to internal resistance can be neglected.

<u>Deployment Site</u>

The sensor system was deployed at Hyalite Creek in Bozeman, MT. This is the site where the Biofilm Structure and Function group's microbial fuel cell has been deployed for the past 4 years. Since there were no detectable levels of metal ion concentration in the creek water, the system was tested by immersing the sensor in a beaker containing water from the creek and adding different amounts of copper and lead.

Current Consumption Determination

The current drawn by the power management circuitry and the potentiostat from the super capacitor has a pulsating nature. This makes it difficult to measure the current consumption by the controller. To calculate the current drawn by the circuitry, an indirect method was used. In this method, the controller was operated by using a charged super capacitor. While the controller was operating, the potential across the super capacitor was logged using the HP 34970A data acquisition/switch unit with a logging interval of 1 second. The current drawn by the controller, at any instant of time during the operation, was calculated using Equation 14 (since the logging interval is 1 sec $\Delta t = 1$). The average current and power drawn by the controller was calculated using Equation 15 and Equation 16, respectively.

$$I_C = \frac{\Delta V}{\Delta t}$$ Equation 14

$$I_{avg} = \frac{\sum I \times t}{\sum t}$$ Equation 15

$$E_{avg} = \frac{\sum V \times I \times t}{\sum t}$$ Equation 16

Runtime of the System

The runtime of the probe was calculated based on the anode lifetime. The lifetime of the magnesium anode used depends on the amount of current drawn

by the controller. Equation 17 was used to calculate the runtime of the controller
developed in this work.

$$t_{lifetime} = \frac{C_{Mg} \times W_{Mg}}{I_{Active} + I_{Sleep}}$$
Equation 17

RESULTS AND DISCUSSION

Figure 18 shows the photograph of the controller that was developed. It was connected to the telemetry system, microbial fuel cell, super capacitor, and sensor before operation.
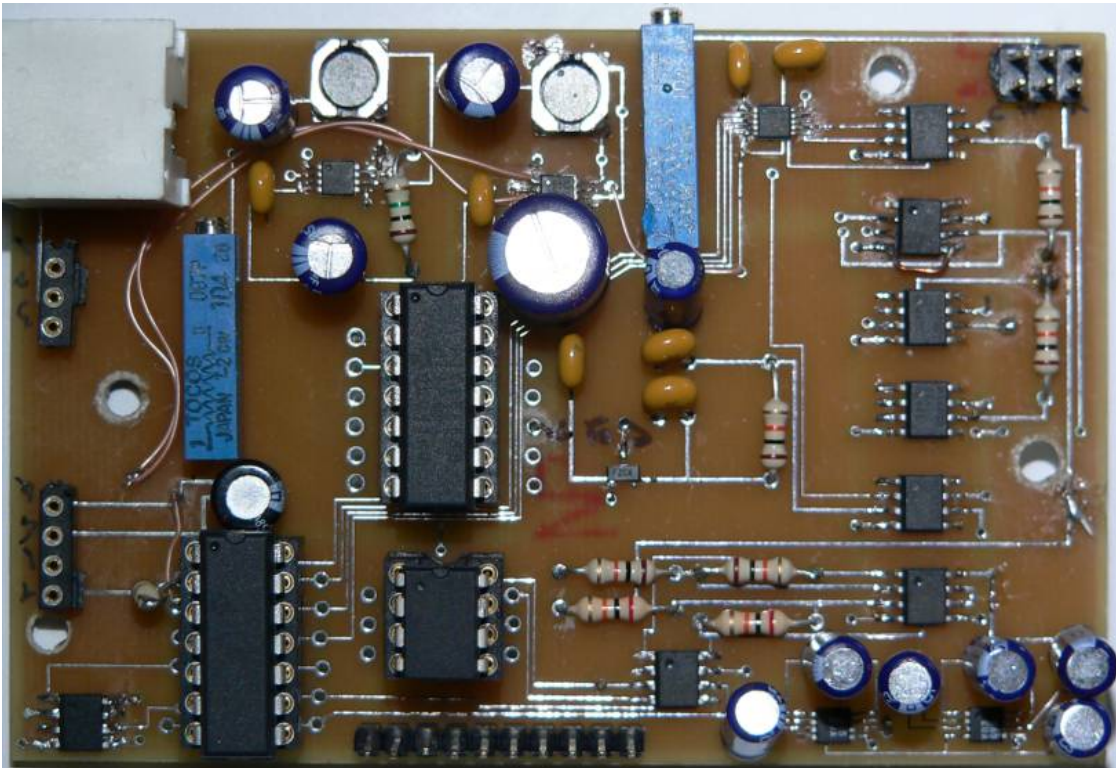
Figure 18. Prototype of the controller.

Figure 19 and Figure 20 show the results of the ASV performed on various known concentrations of copper and lead ion in the creek water, using the commercial (EG&G 273A) potentiostat and the controller, respectively. Both instruments demonstrated similar peaks. The maximum currents for copper and lead were observed at $185mV_{SCE}$ and $-430mV_{SCE}$, respectively. By using the peak current values at these potentials calibrations curves were generated and

are shown in Figure 21 and Figure 22 for lead and copper, respectively. The data

in Figure 21 and Figure 22 demonstrated that the custom designed potentiostat

was able to produce results similar to that of the commercially potentiostat.
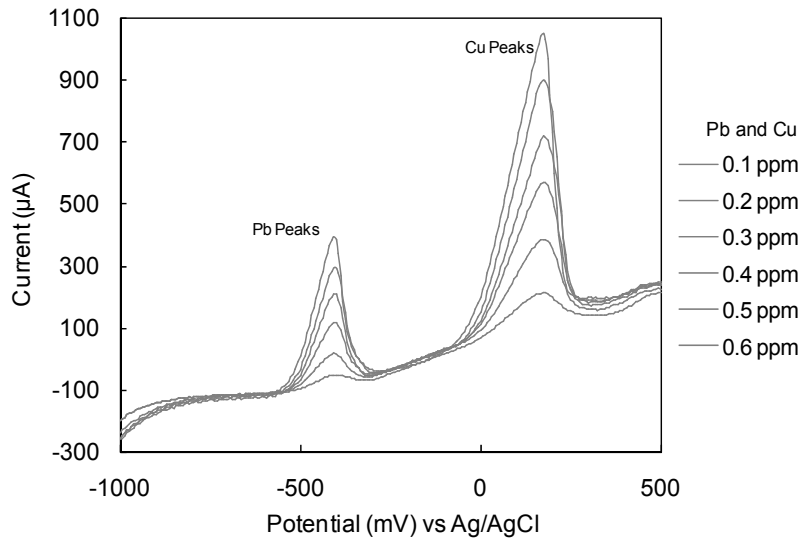
Figure 19. ASV response curves obtained from the commercial potentiostat.
Scan Rate = 25mV/s. Deposition time=60s.
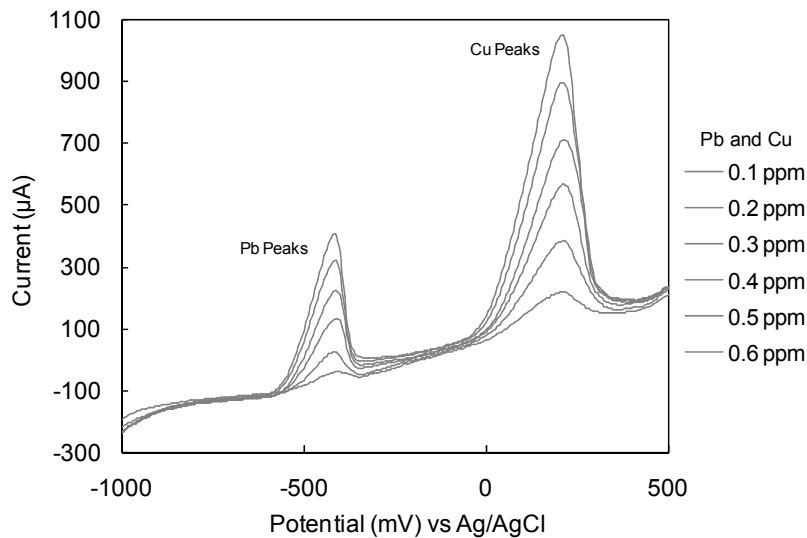
Figure 20. ASV response curves obtained from the custom made sensor
circuitry. Scan Rate = 25mV/s. Deposition time=60s.
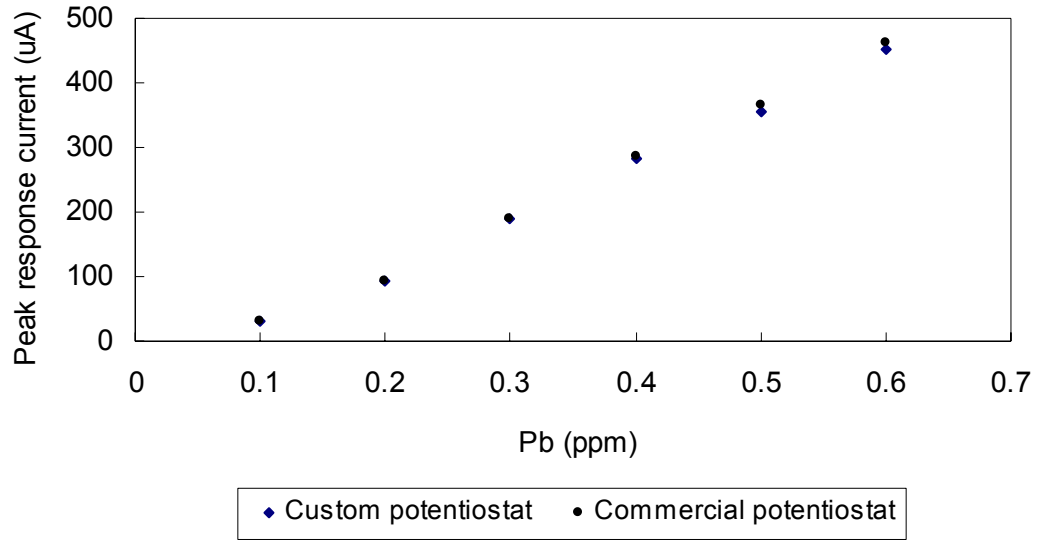
Figure 21. Calibration curves obtained for lead using the commercial potentiostat and the custom made sensor circuitry. The current values were extracted from the lead peaks in Figure 19 and Figure 20. The data points from commercial potentiostat and custom made sensor circuitry overlap.
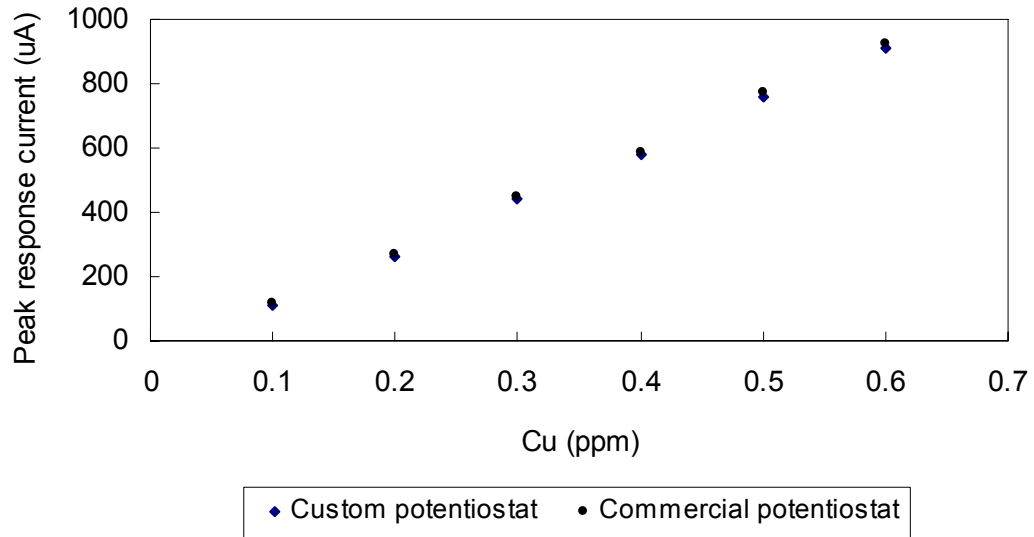
Figure 22 Calibration curves obtained for copper using the commercial potentiostat and the custom made sensor circuitry. The current values were extracted from the copper peaks in Figure 19 and Figure 20. The data points from commercial potentiostat and custom made sensor circuitry overlap.

Figure 23 shows the potential across the capacitor during the deployment of the sensor system in the Hyalite creek. The capacitor was charged using the microbial fuel cell. It took about 42 hrs to charge the capacitor up to a voltage of 1.4V. When a voltage of 1.4V was reached the ASV sequence was started and then the data were transmitted wirelessly. By the end of the wireless transmission the voltage across the capacitor was about 1.2V. It took about 20hrs for the capacitor to be charged back to a voltage of 1.4V. According to the setup used (size of the electrode, capacitor size, transmission power, etc.) a minimum of one transmission per day was achieved.
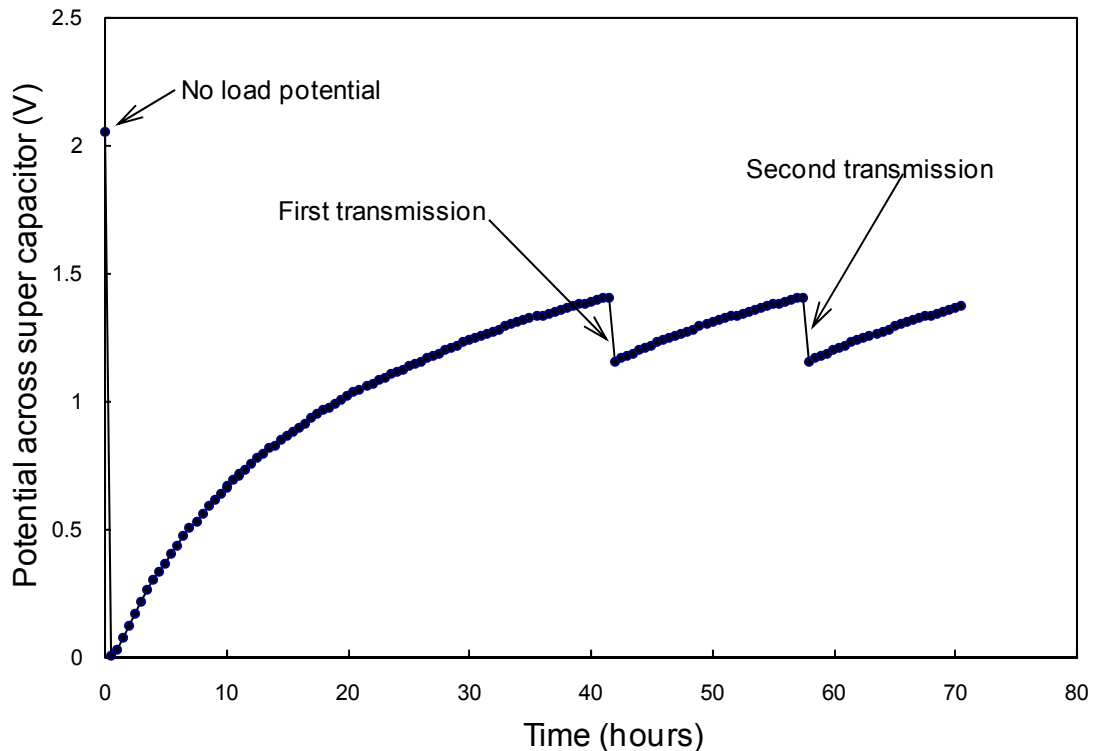
Figure 23. Voltage across the super capacitor connected to the microbial fuel cell and controller during the deployment in the field.

Figure 24 shows the discharge voltage and current of the 350F super capacitor powering the controller. The capacitor potential was 1.4V before being connected to the controller. Using the data from Figure 24 and Equation 16, the average energy consumed by the controller was calculated as 9.3mWh for one complete cycle starting with the deposition until the end of the wireless transmission. The average energy consumed by the controller in the sleep mode was calculated as 1.45µWh. Using Equation 15, the average current consumed by the controller was calculated to be 163mA and 4.4mA while active and in sleep mode, respectively. Using Equation 17 the runtime of the controller powered by the microbial fuel cell was calculated to be 71720 hrs (11.27 years).

Figure 24. Plot of voltage across the capacitor and the current drawn during different functional phases of the controller. Different functional phases of the controller are shown above the time axis.

Implications of the Described System

This research focused on the development of a controller which can be powered by a microbial fuel cell. The electrochemical sensor used in this study was able to measure heavy metal concentration as low as 0.1 ppm. Measuring concentrations of hea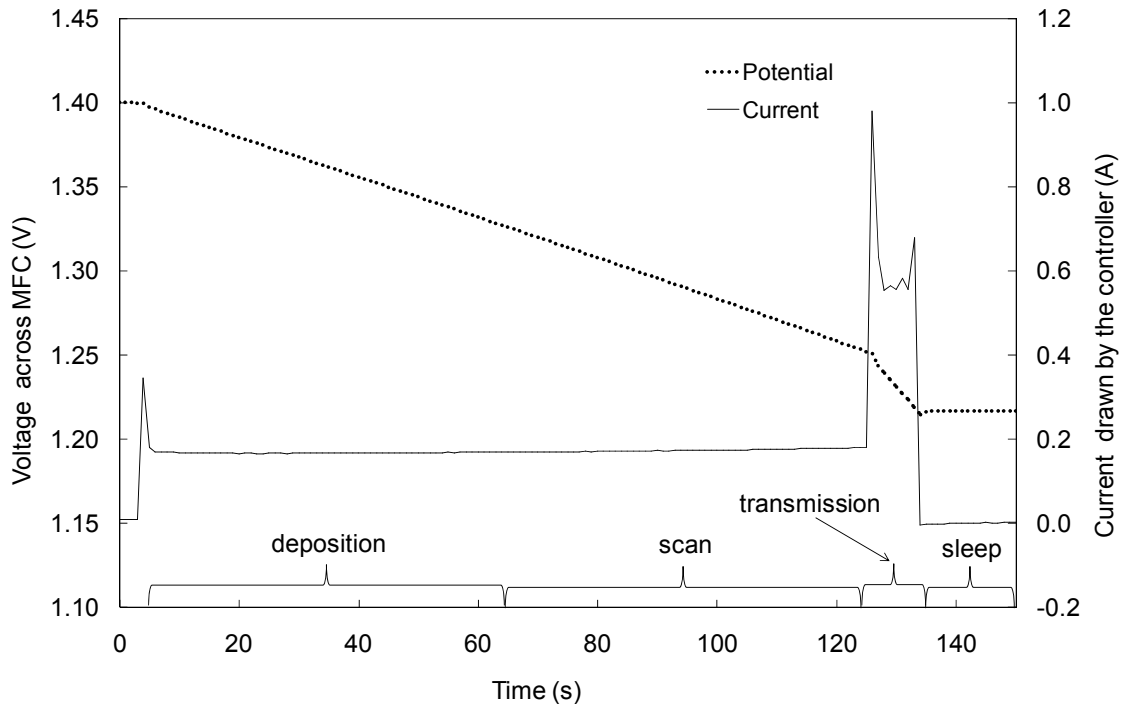vy metals lower than 0.1 ppm can be more attractive since it can help detect early stages of contamination due to heavy metals. Lower concentrations of heavy metals can be measured by using ASV sensor based on microelectrodes [25]. The sensor instrumentation developed in this work can be easily adapted to work with other sensors (microelectrode array, etc.) by changing the gain using VR1 (Figure 9). Thus, measuring lower concentration of heavy metals is still possible by selecting a different sensor while keeping the same system configuration used in this work.

The endurance of the thin film ASV sensors has to be assessed by performing long-term studies. Other research groups are trying to improve the ruggedness of these sensors by coating the thin film mercury with protective membranes [35]. The microbial fuel cell used for testing the sensor system employs a sacrificial magnesium anode. To fully realize the environmentally friendly remote sensor system, it is necessary to power the controller using microbial fuel cells [36-40] which uses microbial reactions at both anode and cathode. Microbial fuel cells using microbial reactions at both anode and cathode develop lower operating voltages than the microbial fuel cell used in this work. A

solution to use the currently designed controller with microbial fuel cells with lower operating voltage is by adding a voltage booster stage to the power management circuitry, based on a charge pump which accepts input voltages as low as 300mV and outputs voltage greater 1V. Another key issue that has to be studied is the effect of back feeding of the current from the super capacitor to the microbial fuel cell. Back feeding of the current into the microbial fuel cell occurs when the voltage of the microbial fuel cell falls lower than the voltage of the super capacitor. Voltage of the microbial fuel cell can go lower than the typical operating voltage depending on various factors such as changes in the microbial activity, resistance of the electrolyte (water system), etc. One of the methods used commonly in electronic circuitry to avoid back feeding is by using a diode. But diodes cannot be used to stop the back feeding of the current to the microbial fuel cell, due to a large voltage drop (0.7V) across the diode.

Conclusions

In this thesis the development and testing of a controller powered by a microbial fuel cell was carried out successfully. The controller was programmed to perform ASV and transmit copper and lead concentration data wirelessly to a base station. The microbial fuel cell powered potentiostat was able to operate identically to a commercially available high power requiring potentiostat. The probe deployed was able to operate and transmit the data to the base station

every 24 hours. The average current consumption of the controller was 163 mA and 4.4 mA in the active and sleep mode, respectively.

Using the controller developed in this work, any generic amperometric sensor can be operated in the field. Since the wireless transmitter used in the controller can transmit over a long distance, the base station can be situated miles away from the sensor deployment site. This facilitates the possibility of deploying many sensors over a large radius surrounding the base station. Modifications to the microcontroller program loaded in the potentiostat and the base station have to be made in order to receive data from multiple controllers using one central base station. By developing the proposed power management circuitry and the potentiostat circuitry, this work has demonstrated that microbial fuel cells can be a solution to the problems associated with the power sources used in the prevailing remote sensors.

REFERENCES CITED

1. Rhoads, A., H. Beyenal, and Z. Lewandowski. "Microbial fuel cell using anaerobic respiration as an anodic reaction and biomineralized manganese as a cathodic reactant." <u>Environmental Science & Technology</u> 39.12 (2005): 4666-71.

2. Shantaram, A. et al. "Wireless sensors powered by microbial fuel cells." <u>Environmental Science & Technology</u> 39.13 (2005): 5037-42.

3. Avinash Shantaram. "Power Management for Microbial Fuel Cells - MS Thesis." <u>Montana State University - Library</u> (2005).

4. Kim, N. et al. "Effect of initial carbon sources on the performance of microbial fuel cells containing Proteus vulgaris." <u>Biotechnology and Bioengineering</u> 70.1 (2000): 109-14.

5. Cooney, M. J. et al. "Physiologic studies with the sulfate-reducing bacterium Desulfovibrio desulfuricans: Evaluation for use in a biofuel cell." <u>Enzyme and Microbial Technology</u> 18.5 (1996): 358-65.

6. Ter Heijne, A., H. V. M. Hamelers, and C. J. N. Buisman. "Microbial fuel cell operation with continuous biological ferrous iron oxidation of the catholyte." <u>Environmental Science & Technology</u> 41.11 (2007): 4130-34.

7. Gil, G. C. et al. "Operational parameters affecting the performance of a mediator-less microbial fuel cell." <u>Biosensors & Bioelectronics</u> 18.4 (2003): 327-34.

8. Min, B. K., S. A. Cheng, and B. E. Logan. "Electricity generation using membrane and salt bridge microbial fuel cells." <u>Water Research</u> 39.9 (2005): 1675-86.

9. Oh, S., B. Min, and B. E. Logan. "Cathode performance as a factor in electricity generation in microbial fuel cells." <u>Environmental Science & Technology</u> 38.18 (2004): 4900-04.

10. Yun, K. S. et al. "A miniaturized low-power wireless remote environmental monitoring system based on electrochemical analysis." <u>Sensors and Actuators B-Chemical</u> 102.1 (2004): 27-34.

11. Steinberg, M. D. and C. R. Lowe. "A micropower amperometric potentiostat." <u>Sensors and Actuators B-Chemical</u> 97.2-3 (2004): 284-89.

12. Kwakye, S. and A. Baeumner. "An embedded system for portable electrochemical detection." <u>Sensors and Actuators B-Chemical</u> 123.1 (2007): 336-43.

13. Serra, P. A. et al. "Design and construction of a low cost single-supply embedded telemetry system for amperometric biosensor applications." <u>Sensors and Actuators B-Chemical</u> 122.1 (2007): 118-26.

14. Beni, V. et al. "Development of a portable electroanalytical system for the stripping voltammetry of metals: Determination of copper in acetic acid soil extracts." <u>Analytica Chimica Acta</u> 552.1-2 (2005): 190-200.

15. Reay, R. J. et al. "Microfabricated electrochemical analysis system for heavy metal detection." <u>Sensors and Actuators B-Chemical</u> 34.1-3 (1996): 450-55.

16. Allen, R. M. and H. P. Bennetto. "Microbial Fuel-Cells - Electricity Production from Carbohydrates." <u>Applied Biochemistry and Biotechnology</u> 39 (1993): 27-40.

17. Batley, G. E. and T. M. Florence. "Evaluation and Comparison of Some Techniques of Anodic-Stripping Voltammetry." <u>Journal of Electroanalytical Chemistry</u> 55.1 (1974): 23-43.

18. Garnier, C. et al. "Voltammetric procedure for trace metal analysis in polluted natural waters using homemade bare gold-disk microelectrodes." <u>Analytical and Bioanalytical Chemistry</u> 386.2 (2006): 313-23.

19. Baldo, M. A. et al. "Remote stripping analysis of lead and copper by a mercury-coated platinum microelectrode." <u>Electroanalysis</u> 16.5 (2004): 360-66.

20. Tanaka, T. et al. "Simultaneous determination of trace copper, lead, cadmium and zinc in iron and steel by stripping analysis." <u>Tetsu to Hagane-Journal of the Iron and Steel Institute of Japan</u> 89.9 (2003): 906-13.

21. Konvalina, J., E. Khaled, and K. Vytras. "Carbon paste electrode as a support for mercury film in potentiometric stripping determination of heavy metals." <u>Collection of Czechoslovak Chemical Communications</u> 65.6 (2000): 1047-54.

22. Matysik, F. M. and G. Werner. "Trace-Metal Determination in Tears by Anodic-Stripping Voltammetry in A Capillary-Flow Injection System." <u>Analyst</u> 118.12 (1993): 1523-26.

23. Larry R.Faulkner and Allen J.Bard. "Electrochemical Methods: Fundamentals and Applications." <u>Wiley.ISBN: 978-0-471-04372-0</u> (2004).

24. Florence, T. M. "Anodic Stripping Voltammetry with A Glassy Carbon Electrode Mercury-Plated In-Situ." <u>Journal of Electroanalytical Chemistry</u> 27.2 (1970): 273-&.

25. Wehmeyer, K. R. and R. M. Wightman. "Cyclic Voltammetry and Anodic-Stripping Voltammetry with Mercury Ultramicroelectrodes." <u>Analytical Chemistry</u> 57.9 (1985): 1989-93.

26. Data sheet: MAX54444 +3V/+5V, Serial-Input, Voltage-Output, 16-Bit Digital to Analog Converters. <u>Maxim Integrated Products</u> *Rev 1; 6/01* (2001).

27. Data sheet: MAX1797 Low Supply Current, Step-Up DC-DC Converters with True-Shutdown. <u>Maxim Integrated Products</u> 19-1798; Rev 0; 12/00 (2000).

28. Data sheet: MAX865 Compact, Dual-Output Charge Pump. <u>Maxim Integrated Products</u> 19-0472; Rev 1; 7/97 (1997).

29. Data sheet: MAX400 Ultra-Low Offset Voltage Operational Amplifier. <u>Maxim Integrated Products</u> 19-3001; Rev 1; 12/03 (2003).

30. Data sheet: OPA2350 - High-Speed, Single-Supply, Rail-to-Rail OPERATIONAL AMPLIFIERS MicroAmplifierSeries. <u>Texas Instruments</u> SBOS099C (2005).

31. Data sheet: ADC1252 - 24-Bit, 40kHz ANALOG-TO-DIGITAL CONVERTER. <u>Texas Instruments</u> SBAS127D (2006).

32. Data sheet: PIC16F688 14-Pin Flash-Based, 8-Bit CMOS Microcontrollers with nanoWatt Technology. <u>Microchip Technology Inc.</u> DS41203B (2004).

33. Data sheet: PIC12F629/675 14-Pin Flash-Based, 8-Bit CMOS Microcontrollers with nanoWatt Technology. <u>Microchip Technology Inc.</u> DS41190C (2003).

34. Data sheet: 25AA320/25LC320/25C320 - 32K SPI™ Bus Serial EEPROM. Microchip Technology Inc. DS21227E (2004).

35. Hoyer, B., T. M. Florence, and G. E. Batley. "Application of Polymer-Coated Glassy-Carbon Electrodes in Anodic-Stripping Voltammetry." Analytical Chemistry 59.13 (1987): 1608-14.

36. He, Z., H. B. Shao, and L. T. Angenent. "Increased power production from a sediment microbial fuel cell with a rotating cathode." Biosensors & Bioelectronics 22.12 (2007): 3252-55.

37. Lowy, D. A. et al. "Harvesting energy from the marine sediment-water interface II - Kinetic activity of anode materials." Biosensors & Bioelectronics 21.11 (2006): 2058-63.

38. Ryckelynck, N., H. A. Stecher, and C. E. Reimers. "Understanding the anodic mechanism of a seafloor fuel cell: Interactions between geochemistry and microbial activity." Biogeochemistry 76.1 (2005): 113-39.

39. Tender, L. M. et al. "Harnessing microbially generated power on the seafloor." Nature Biotechnology 20.8 (2002): 821-25.

40. Reimers, C. E. et al. "Harvesting energy from the marine sediment-water interface." Environmental Science & Technology 35.1 (2001): 192-95.